Endothelial Rbpj is essential for the education of tumour-associated macrophages

Ronja Mülfarth[1,2*], Elisenda Alsina-Sanchis[1*], Iris Moll[1], Sarah Böhn[1], Lena Wiedmann[1,2,] Lorea Jordana[1], Tara Ziegelbauer[1], Jacqueline Taylor[1], Francesca De Angelis Rigotti[1,3], Adrian Stögbauer[1], Benedetto Daniele Giaimo[4], Adelheid Cerwenka[5,6], Tilman Borggrefe[4], Andreas Fischer[1,5,7,*], Juan Rodriguez-Vita[1,3,*]

[1]Division Vascular Signaling and Cancer, German Cancer Research Center (DKFZ), 69120 Heidelberg, Germany.

[2]Faculty of Biosciences, University of Heidelberg, 69120 Heidelberg, Germany.

[3]Tumour-Stroma Communication Laboratory, Centro de Investigación Príncipe Felipe, 46012 Valencia, Spain.

[4]Institute of Biochemistry, University of Giessen, 35392 Giessen, Germany.

[5]European Center for Angioscience (ECAS), Medical Faculty Mannheim, University of Heidelberg, 68167 Mannheim, Germany.

[6]Department of Immunobiochemistry, Mannheim Institute for Innate Immunoscience (MI3), Medical Faculty Mannheim, University of Heidelberg, 68167 Mannheim, Germany

[7]Institute for Clinical Chemistry, University Medical Center Göttingen, 37075 Göttingen, Germany.

* Equal contribution.

Correspondence to: a.fischer@dkfz.de, jrodriguez@cipf.es

1 **Abstract**

2 Epithelial ovarian cancer (EOC) is one of the most lethal gynaecological cancers worldwide.

3 EOC cells educate tumour-associated macrophages (TAMs) through CD44-mediated

4 cholesterol depletion to generate an immunosuppressive tumour microenvironment (TME).

5 In addition, tumour cells frequently activate Notch1 receptors on endothelial cells (ECs) to

6 facilitate metastasis. However, little is known whether the endothelium would also influence

7 the education of recruited monocytes. Here, we report that canonical Notch signalling

8 through RBPJ in ECs is an important player in the education of TAMs and EOC progression.

9 Deletion of *Rbpj* in the endothelium of adult mice reduced infiltration of monocyte-derived

10 macrophages into the TME of EOC and prevented the acquisition of a typical TAM gene

11 signature. This was associated with stronger cytotoxic activity of T cells and decreased

12 tumour burden. Mechanistically, we identified CXCL2 as a novel Notch/RBPJ target gene.

13 This angiocrine factor regulates the expression of CD44 on monocytes and subsequent

14 cholesterol depletion of TAMs. Bioinformatic analysis of ovarian cancer patient data showed

15 that increased CXCL2 expression is accompanied by higher expression of CD44 and TAM

16 education. As such, EOC cells employ the tumour endothelium to secrete CXCL2 in order to

17 facilitate an immunosuppressive microenvironment**.**

18

19 **Introduction**

20 High grade serous ovarian cancer is the deadliest type of all gynaecological

21 cancers[1]. The high mortality rate is due to the fact that most women have already developed

22 peritoneal metastasis at the time of diagnosis. Epithelial ovarian cancer (EOC) cells can

23 directly infiltrate the peritoneal cavity to seed metastases, a process called transcoelomic

24 metastasis[2]. Metastatic EOC cells initially reside in the omentum, where they undergo

25 certain adaptations allowing them to spread throughout the whole peritoneal cavity.

Importantly, this peritoneal microenvironment is so immunosuppressive that even the infiltration of effector T cell does not *per se* correlate with better prognosis[3].

Peritoneal spread of tumour cells is accompanied by monocyte-derived macrophage (MN-derived macrophages) recruitment, which eventually become the most abundant myeloid cell type[4] and are a major contributor to the immunosuppressive TME in EOC[3]. Upon recruitment from blood to the tumour, monocytes differentiate into macrophages which are further educated by the TME. Eventually, tumour-associated macrophages (TAMs) strongly promote the progression of metastatic ovarian cancer[5]. However, little is known about the contribution of other stromal cells to the peritoneal spread of EOC cells and to macrophage education.

Monocytes must cross the vascular endothelial barrier before infiltrating peritoneal organs or the peritoneal fluid. Endothelial cells (ECs) not only form tubes for the transport of blood, but also produce soluble factors controlling the differentiation and function of adjacent cells. These angiocrine functions are highly context and organ specific[6,7]. In cancer, ECs provide angiocrine factors which influence tumour progression[8]. Therefore, we hypothesized that monocytes are influenced by ECs, for instance during transmigration, while infiltrating into peritoneal tissues.

Notably, tumours can alter the transcriptome of ECs[9,10] and this may also influence transmigrating monocytes. For example, endothelial Notch signalling activity is frequently higher in tumours like EOC and in the metastatic niche compared to ECs from non-tumourous tissue[11]. Notch signalling is a highly conserved cell-to-cell communication system. Ligand binding induces cleavage of the transmembrane Notch receptors releasing the intracellular domain (ICD) which enters the nucleus to alter gene transcription. This canonical signalling pathway relies on the DNA-binding protein RBPJ, which turns into a transcriptional activator upon binding of a Notch receptor ICD[12]. Sustained endothelial Notch1 signalling is associated with increased myeloid cell infiltration and metastasis[11]. The Notch pathway in ECs is a major regulator of angiogenesis, metabolism, angiocrine

1   functions and tumour cell transmigration[11,13-18]. Although EOC cells do not necessarily have

2   to cross the endothelial barrier to spread throughout the peritoneum we hypothesized that

3   endothelial Notch signalling could still influence EOC progression via transmigrating myeloid

4   cells.

5   Here, we provide insights into the essential role of RBPJ in ECs for the recruitment of

6   monocytes to the microenvironment of metastatic EOC and their proper education into pro-

7   tumoural TAMs.

8

9   **Results**

10   **Deletion of *Rbpj* in endothelial cells reduces EOC progression**

11   Metastatic EOC cells seed initially in the omentum and later spread within the

12   peritoneum. During these steps, tumour cells undergo transcriptional changes that allow

13   them to further grow and colonise (**Fig. 1a**). The latter is strongly influenced by MN-derived

14   macrophages[19]. To determine the contribution of canonical Notch signalling in ECs to

15   myeloid cell infiltration and EOC progression, we used the tamoxifen-inducible VE-Cadherin

16   (Cdh5) Cre^{ERT2} strain to delete *Rbpj* specifically in ECs of adult mice (*Rbpj*$^{i\Delta EC}$). This mouse

17   model is well established and leads to robust gene recombination in ECs of several

18   organs[14,15,17,18] (**Fig. 1b**). Under physiological conditions, there were no differences in blood

19   vessel density in the larger omentum upon *Rbpj* deletion in ECs compared to controls

20   (**Suppl. Fig. 1a,b**). However, upon intraperitoneal injection of ID8 cells mimicking metastatic

21   EOC, the omenta showed evidence of tumour nodule growth (**Fig. 1c**) and had significantly

22   higher vessel density in *Rbpj*$^{i\Delta EC}$ mice compared to control animals (**Fig. 1d**). The density of

23   endothelial coverage with α-smooth muscle actin-positive mural cells was, however,

24   unchanged (**Suppl. Fig. 1c**). Despite increased vessel density, tumour burden in omenta of

25   *Rbpj*$^{i\Delta EC}$ mice was significantly lower than that in their littermate controls (**Fig. 1e**). Moreover,

4

1   peritoneal spread of tumour cells was significantly reduced as well in $Rbpj^{i\Delta EC}$ mice (**Fig. 1f**)

2   concluding that deletion of $Rbpj$ in ECs reduces EOC progression and metastasis.

3

4   **Deletion of endothelial *Rbpj* decreases monocyte-derived macrophage recruitment**

5   Next, we analysed the immune cell compartment of our EOC model since it is a

6   major contributor to tumour progression. High Notch signalling activity in ECs induces

7   VCAM1 expression, which promotes leukocyte extravasation[11,20]. However, VCAM1

8   expression was unchanged between $Rbpj^{i\Delta EC}$ and their controls littermates (**Suppl. Fig. 2a**).

9   Nevertheless, whole-mount staining of omenta revealed that there was a reduction in

10   immune cells inside tumour nodules of $Rbpj^{i\Delta EC}$ mice compared to controls (**Fig. 2a** and

11   **Suppl. Fig. 2b**). Interestingly, tumours in control mice contained more cells with a large

12   vacuolated cytoplasm, reminiscent of macrophages. Therefore, we analysed this cell

13   population in greater detail. Tumour-bearing omenta from $Rbpj^{i\Delta EC}$ mice contained less

14   $CD11b^+$ cells within tumour nodules, although this reduction was not statistically significant

15   (**Fig. 2b**). In order to better determine the macrophage subpopulations responsible for the

16   observed decrease in $CD11b^+$ cells; we studied the myeloid and macrophage populations in

17   the peritoneal cavity to understand whether RBPJ in ECs could play a role in their

18   composition. After four weeks of tumour growth, there were no significant differences in the

19   total amount of myeloid cells or macrophages (**Fig. 2c,d**). However, we found decreased

20   numbers of small peritoneal macrophages (SPMs), which are MN-derived macrophages

21   characterized as MHC-II^{hi}/F4/80^{low} (**Fig. 2e**) and CCR2$^+$/Tim4$^-$ (**Fig. 2f**). Notably, in naïve

22   (tumour-free) conditions, endothelial $Rbpj$ deletion had no effect on peritoneal macrophage

23   populations (**Suppl. Fig. 2c-f**). These data suggest that the tumour-driven recruitment of

24   monocytes into the peritoneum is impaired upon endothelial deletion of $Rbpj$.

25   To further dissect endothelial chemotaxis in a more simplified *in vitro* system, we

26   switched to the human system and measured transmigration of human $CD14^+$ monocytes

5

1   through a monolayer of human ECs in a transwell insert. Chemotaxis was stimulated by SK-

2   OV-3 human ovarian cancer cells below the insert (**Fig. 2g**). *RBPJ* deletion in human

3   umbilical vein ECs (HUVECs) resulted in significantly decreased monocyte transmigration

4   rates compared to control HUVECs (**Fig. 2h**). This further suggests that canonical Notch

5   signalling in ECs is important to facilitate monocyte recruitment into the TME.

6

7   **Canonical Notch signalling in ECs regulates monocyte recruitment through CXCL2**

8   We have previously analysed the transcriptional induction of chemokines in HUVECs

9   upon Notch1 ICD (N1ICD) overexpression[11]. Based on this, we transduced *RBPJ*-deficient

10   HUVEC and control cells with N1ICD to determine which of those transcriptional changes

11   require *RBPJ*. The chemokines that were induced by N1ICD through RBPJ were *CCL1,*

12   *CCL21, CXCL12,* and *CXCL2* (**Fig. 3a**) and we excluded those that were not induced

13   through RBPJ (**Suppl. Fig. 3a-b**). Next, we measured the mRNA expression levels of these

14   chemokines in peritoneal adipose tissue obtained from *Rbpj*$^{i\Delta EC}$ mice. This revealed that

15   there was lower *Cxcl2* expression in peritoneal adipose tissue from *Rbpj*$^{i\Delta EC}$ mice compared

16   to littermate controls, whereas the other chemokines analysed were not changed (**Fig. 3b**).

17   Analysis of the same cytokines in endothelial-specific N1ICD mice[11,15], exposed that higher

18   endothelial Notch1 signalling activity led to higher *Cxcl2* expression in peritoneal adipose

19   tissue (**Fig. 3c**).

20   *In silico* analysis showed that the mouse and human *Cxcl2* gene contains RBPJ-

21   binding sites in the promoter region (**Fig. 3d**). Consistently, cultured human ECs secreted

22   higher CXCL2 protein levels after being transduced with N1ICD expressing adenovirus

23   compared to GFP-transduced control cells (**Fig. 3e**).

24   These data revealed that canonical Notch signalling induces CXCL2 expression in

25   ECs. CXCL2 is known to attract granulocytes but also to a lesser extend monocytes[21]. As

26   such, it poses as an interesting endothelial Notch target, which could mediate the observed

1   effects on monocyte recruitment into the TME. To evaluate whether CXCL2 was capable of

2   attracting monocytes, we performed transwell chemotaxis experiments and observed that

3   recombinant CXCL2 induced monocyte chemotaxis (**Fig. 3f**). Next, we silenced *CXCL2*

4   expression in ECs using shRNA, which led to an about 50% reduction of CXCL2 protein

5   expression (**Fig. 3g**). Compared to non-silencing control, this reduction of CXCL2 levels was

6   already capable of reducing the numbers of monocytes transmigrating through ECs towards

7   SK-OV-3 cells (**Fig. 3h**). In summary, the data implicate that the endothelial RBPJ/CXCL2

8   axis contributes to monocyte recruitment into the peritoneum during transcoelomic

9   metastasis.

10

11   ***Rbpj* in ECs is necessary for tumour-mediated TAM education**

12   Recruited monocytes differentiate into macrophages which are further educated by

13   tumour cells to become tumour-promoting macrophages. Macrophage education in EOC is

14   facilitated by hypersensitivity towards IL4, which is induced by tumour cell-mediated

15   cholesterol depletion[4]. We sought to understand whether lack of *Rbpj* in ECs could influence

16   macrophage phenotypes. To assess this, we isolated newly recruited MN-derived

17   macrophages (CD11b$^+$/F4/80$^+$/CCR2$^+$) (**Fig. 4a**) and obtained their transcriptomic profile by

18   microarray analysis. Gene set enrichment analysis (GSEA) comparing MN-derived

19   macrophages from *Rbpj*$^{i\Delta EC}$ and control tumour-bearing mice revealed that *Rbpj* in ECs is

20   necessary to acquire the typical phenotype of TAM in this model of metastatic EOC (**Fig.**

21   **4b**). As such, tumour cells could not fully educate MN-derived macrophages in mice lacking

22   endothelial *Rbpj.*

23   Transcriptomic profiling via Ingenuity Pathway Analysis (IPA) determined that IL4

24   was the most downregulated signalling pathway in MN-derived macrophages obtained from

25   *Rbpj*$^{i\Delta EC}$ tumour bearing mice (**Fig. 4c**). IPA and pathway analysis showed that genes

26   important for cholesterol synthesis were downregulated in MN-derived macrophages from

27   *Rbpj*$^{i\Delta EC}$ mice (**Fig. 4d,e**). We then employed a cholesterol homeostasis gene set from TAMs

7

1   obtained 21 days after tumour injection[4], representing EOC-induced cholesterol metabolism

2   in TAMs. GSEA showed that this gene set was significantly enriched in newly recruited

3   macrophages coming from control tumour-bearing mice (**Fig. 4f**), indicating that *Rbpj* in ECs

4   is necessary for cholesterol depletion in TAMs.

5   Cholesterol depletion is mediated by tumour cell-secreted high molecular weight

6   hyaluronan (HMW-HA). The interaction with HA receptors, such as CD44, in macrophages

7   leads to cholesterol efflux through ABC transporters[4]. In order to understand whether *Rbpj* in

8   ECs could be important for CD44 expression in monocytes, we co-cultured human

9   monocytes with HUVECs lacking *RBPJ* or with respective controls. Monocytes co-cultured

10   with *RBPJ*-deficient HUVECs, had less CD44 on their membrane than those incubated with

11   control HUVECs (**Fig. 4g**). Next, when incubating bone marrow-derived macrophages

12   (BMDMs) with conditioned medium (CM) from immortalized mouse cardiac endothelial cells

13   (MCECs) lacking *Rbpj* (CRISPR-Cas9 mediated), macrophages expressed less *Cd44* (**Fig.**

14   **4h**) and *Mmp9* (**Fig. 4i**), a known CD44 target gene. This indicates that a secreted

15   angiocrine factor regulated by the transcription factor RBPJ in ECs is necessary for the

16   regulation of CD44 in macrophages. To understand whether this would also happen *in vivo*,

17   *Rbpj*[iΔEC] and control mice were injected with thioglycolate to induce MN-derived macrophage

18   recruitment in the absence of tumour cells. We found that MN-derived macrophages in

19   *Rbpj*[iΔEC] mice expressed significantly less *Cd44* than those in control mice (**Fig. 4j**),

20   confirming that RBPJ in EC is essential for *Cd44* regulation in MN-derived macrophages *in*

21   *vivo*.

22   Considering the important role that CXCL2 had in monocyte recruitment in *Rbpj*[iΔEC]

23   tumour bearing mice and that higher level of CXCL2 in serum is associated not only with

24   myeloid cell infiltration into the TME, but also with worse prognosis for EOC patients[22], we

25   decided to analyse its role in regulating CD44 expression. Indeed, when stimulating BMDMs

26   with CXCL2, *Cd44* expression was increased (**Fig. 4k**). Moreover, since CD44 is a

27   membrane-bound receptor, we analysed by immunofluorescence whether also its cellular

28   localization could be altered. We observed that CXCL2 stimulation of BMDMs increased the

8

1   presence of CD44 on the plasma membrane, which would consequently increase its

2   accessibility to hyaluronic acid (**Fig. 4I** and **Suppl. Fig. 4**).

3

4   **The TAM gene signature is enriched in human ovarian carcinoma samples with high**

5   **CXCL2 expression**

6   The data presented so far indicate that the angiocrine factor CXCL2, which is under

7   transcriptional control of Notch/RBPJ signalling, preconditions monocytes to be educated by

8   tumour cells in the TME. In order to evaluate the relevance of this, we analysed *CXCL2* and

9   *CD44* mRNA expression levels in publicly available data sets from the Cancer Genome Atlas

10   (TCGA). Remarkably, the stratification of ovarian cancer patients in 25% upper (CXCL2^{hi})

11   and lower (CXCL2^{low}) *CXCL2* expression showed that CXCL2^{hi} patients displayed

12   significantly more expression of *CD44* (**Fig. 5a**). These data suggest a positive correlation

13   between *CXCL2* and *CD44* expression in human tumours. Our data indicate that CXCL2-

14   mediated CD44 induction reflects the ability of tumour cells to educate TAMs. Therefore, the

15   correlation in expression between CXCL2 and CD44 should in turn have implications on

16   TAM education. Therefore, we performed GSEA comparing CXCL2^{hi} and CXCL2^{low} patients

17   using the abovementioned TAM signature. We observed that the TAM signature was

18   significantly enriched in CXCL2^{hi} patients (**Fig. 5b**), indicating that the increased CD44

19   expression in these patients consequently impacts TAM education.

20   When analysing difference between CXCL2^{hi} and CXCL2^{low} patients, we found an

21   expected upregulation of chemotactic response and myeloid cell recruitment, as shown by

22   gene ontology (GO) term analysis in CXCL2^{hi} patients (**Suppl. Fig. 5**), supporting the role of

23   CXCL2 in controlling the myeloid cell compartment of tumours. Interestingly, we again

24   identified cholesterol metabolism as one of the most downregulated pathways in CXCL2^{low}

25   patients (**Fig. 5c**). Instead, CXCL2^{hi} patients showed induction of pathways such as lipid and

26   atherosclerosis, thus suggesting opposite profiles (**Fig. 5d**). Indeed, GSEA showed that the

1   same cholesterol metabolism gene set previously employed was significantly enriched in

2   CXCL2^{hi} cohort (**Fig. 5e**), indicating a similar cholesterol depletion as the one occurring in

3   peritoneal macrophages of our mouse model.

4

5   **TAM education mediated by endothelial *Rbpj* affects T cell cytotoxicity**

6   One of the genes downregulated in MN-derived macrophages from *Rbpj*^{iΔEC} tumour-

7   bearing mice is *Cd74* (**Fig. 4b**). CXCL2 is a ligand for CXCR2[21], and CD44 is part of a

8   receptor complex that contains CD74 and CXCR2[23,24]. Moreover, CD44 plays an important

9   role in CD74-mediated signal transduction[25]. *In silico* analysis showed that CD74 interacts

10   closely with CD44 and CXCR2 (**Fig. 6a**). Besides, CD74 has been reported to be important

11   in TAMs in brain metastasis[26], and CD74 expression has been associated with worse

12   prognosis in metastatic ovarian cancer[27]. Furthermore, CD74 was associated with an

13   immunosuppressive phenotype in macrophages[28]. We decided to investigate whether the

14   downregulation of CD74 could have a consequence on TAM behaviour. For that, we

15   analysed publicly available data sets where IL4 responses in CD74-deficient macrophages

16   were analysed[29]. GSEA showed that TAM signature was enriched in wild-type macrophages,

17   indicating that CD74 is not only regulated by IL4, but also necessary for TAM education (**Fig.**

18   **6b**). We extracted a signature with the 500 most enriched genes in control compared to

19   CD74-deficient macrophages stimulated with IL4 (CD74-mediated signature), representing a

20   group of genes induced by IL4 through CD74 activation. When comparing newly recruited

21   MN-derived macrophages from our EOC model by GSEA, we found that the CD74-mediated

22   signature was significantly enriched in macrophages isolated from control mice compared to

23   *Rbpj*^{iΔEC}. This suggests that newly recruited macrophages from *Rbpj*^{iΔEC} mice cannot induce

24   their immunosuppressive phenotype due to downregulation of CD74-mediated genes (**Fig.**

25   **6c**).

1   To verify the specific effect on the newly recruited macrophages, we repeated the

2   same analysis on resident macrophages (CD11b$^+$/F4/80$^+$/CCR2$^-$), in which *Cd74* is not

3   differentially expressed between *Rbpj*$^{i\Delta EC}$ tumour-bearing and control mice, and found no

4   enrichment of this gene set in any group, confirming that *Rbpj* deletion in ECs only affects

5   *Cd74* expression in newly recruited MN-derived macrophages (**Suppl. Fig. 6**). In summary,

6   only macrophages that have crossed the EC barrier as monocytes were affected by the lack

7   of *Rbpj* in the endothelium.

8   It has been previously reported that TME in metastatic ovarian cancer is highly

9   immunosuppressive and infiltration with immune effector cells has little impact in patients'

10 outcome[3]. This immunosuppressive microenvironment has been attributed to TAMs[3]. For

11 this reason, we wanted to test whether impaired TAM education could impact on the

12 phenotype of the TME. We isolated T cells from tumour-bearing *Rbpj*$^{i\Delta EC}$ mice and their

13 littermate controls six weeks after intraperitoneal injection of ID8 cells (**Fig. 6d**). Results

14 demonstrated that T cells derived from *Rbpj*$^{i\Delta EC}$ mice were more efficient in killing cultured

15 ID8 cells (**Fig. 6e**). This confirms that impairment in TAM education has a direct impact on T

16 cell cytotoxicity. In addition, the analysis of T cell populations in peritoneal cavity from

17 tumour-bearing mice revealed that, although the total frequency of T cells was not changed,

18 the cytotoxic CD8$^+$ T cell population was significantly increased in *Rbpj*$^{i\Delta EC}$ mice compared to

19 their littermate controls (**Fig. 6f**). In summary, our data reveal that *Rbpj* in ECs is necessary

20 for tumour cell-mediated education of MN-derived macrophages into TAMs (**Fig. 6g**).

21

22 **Discussion**

23 Collectively, this study provides evidence about a novel angiocrine axis influencing

24 the tumour immune microenvironment. We show how Notch/RBPJ-mediated transcription in

25 ECs, which is frequently hyperactive in tumours[11], is required for CXCL2-mediated monocyte

1   chemotaxis, induction of CD44 expression on monocytes, and the adoption of a TAM gene

2   signature in metastatic ovarian cancer.

3   Mice with EC-restricted *Rbpj loss* had impaired ovarian carcinoma growth in the

4   omentum and peritoneum and lower numbers of MN-derived macrophages in the peritoneal

5   fluid. These macrophages are essential for metastatic ovarian cancer development[4,30]. As

6   such, the endothelium can influence tumour progression and metastasis by altering the

7   immune status of the TME. Specifically, we observed that monocyte recruitment is

8   potentiated, at least in part, through the release of *Rbpj*-mediated CXCL2 from ECs.

9   Interestingly, higher serum levels of CXCL2 in ovarian cancer patients are associated with

10   myeloid cell infiltration, poor prognosis and chemoresistance[31]. It should be noted that this

11   chemokine has been traditionally associated with the recruitment of neutrophils[21]. However,

12   there is evidence that CXCL2 also plays a role in the regulation of TAMs, especially those

13   derived from monocytes. For instance, the CXCL2 receptor CXCR2 on monocytes and

14   macrophages is important for the education of TAMs in prostate cancer[32].

15   CXCR2 blockade has also been shown to re-sensitize ovarian cancer to cisplatin

16   treatment[33]. Here we suggest that the CXCL2/CXCR2 axis might also have a role in the

17   recruitment and education of macrophages in ovarian cancer. By separating newly recruited

18   macrophages from macrophages that have reside in the peritoneal cavity for a longer period,

19   we observed that endothelial RBPJ is necessary for the education into TAMs by tumour

20   cells. Specifically, we report that MN-derived macrophages in contact with ECs lacking RBPJ

21   had a lower expression of the HA receptor CD44. This receptor gets stimulated by HMW-HA

22   produced by tumour cells to induce cholesterol depletion in macrophages, a crucial

23   mechanism by which tumour cells educate TAMs[4]. Therefore, we propose that through this

24   mechanism ECs can pre-condition MN-derived macrophages and contribute to their

25   immunosuppressive phenotype within the tumour microenvironment. Indeed, the data

26   showed that important genes involved in cholesterol depletion were reduced in MN-derived

27   macrophages from mice lacking RBPJ in their ECs. Consistently, T cells isolated from this

TME were more efficient at killing tumour cells, confirming the reduced immunosuppressive potential of the MN-derived macrophages.

In conclusion, we demonstrate that peritoneal ECs are critically involved in the recruitment and education of MN-derived macrophages in ovarian carcinoma.

Material and methods

Animal models

All animal procedures were approved by the local institutional animal care and use committee (RP Karlsruhe, Germany and DKFZ) and performed according to the guidelines of the local institution and the local government. Female C57BL/6 mice were group-housed under specific pathogen-free barrier conditions.

Administration of tamoxifen diluted in sterile peanut (P2144, Sigma-Aldrich, St. Louis, USA) in 8 to 12-week-old randomized mice was performed by oral gavage once with 100 µl (1 mg tamoxifen)[34]. Control mice, which did not express Cre^{ERT2} were also treated with tamoxifen.

Model of ovarian cancer: Three weeks after gene recombination, 5×10^6 ID8-luciferase (ID8-luc) ovarian cancer cells were administered i.p. in PBS. For peritoneal lavage after sacrificing the mice, 5 ml of ice-cold PBS (Gibco/Thermo Fisher Scientific, NY, USA) was injected i.p., and after a careful massage to mobilize cells, peritoneal fluid was collected. For analysis of ID8-luc tumour growth the cell suspension was centrifuged and supernatant was collected. The cell pellet was suspended in 1 mL PBS and 100 µL were used to determine the luciferase activity. 100 µL cell suspension were centrifuged and the cell pellet was suspended in 100 µL lysis buffer (Promega) and 20 µL of lysed cells were pipetted into white 96-well plate in triplicates. 50 µL of LAR substrate (Promega) was added to the lysed cell suspension and luminescence signal was determined using the plate reader (ClarioStar,

BMG Labtech). For analysis of immune cell recruitment into the peritoneal cavity the collected peritoneal cell suspension was centrifuged and red blood cells in the cell pellet were lysed with 1 mL ACK (Thermo Fisher Scientifics). After washing the cell suspension was counted using Neubauer Counting chamber and 1×10^6 cells were used for flow cytometry staining.

Model of peritoneal inflammation: To obtain newly recruited peritoneal macrophages, 1 mL thioglycolate (2 mg/mL in H_2O; B2551, Sigma-Aldrich) was injected into the peritoneum three weeks after gene recombination. MN-derived macrophages were isolated 24 hours after thioglycolate injection by their adherence to non-treated plastic petri dishes. Briefly, after incubation of single cells in a petri dish for 30 min at 37C, non-adherent cells washed away with PBS.

Flow cytometry

For flow cytometry analysis, cells were suspended in 1 mL PBS with 2% FCS (Biochrom). Cell suspension was incubated with the different fluorophore-coupled primary antibodies for 20 min on ice. The following antibodies were used: CD45 (552848), CD11b (552850) and CD4 (560468) and CD8 (557654) from BD Biosciences (Bedford, MA, USA); CD3 (100203), F4/80 (123128), CCR2 (150608), CD44 (mouse and human 103007), CD74 (mouse (151005) and human (326811)) from BioLegend (St. Diego, CA, USA), MHCII (47-5321-80, Life Technologies/Thermo Fisher Scientific, NY, USA) and Tim4 (12-5866-82, Life Technologies/Thermo Fisher Scientific, NY, USA). Concentration of the different antibodies was determined by titration. In the meanwhile, compensation beads (UltraComp eBeads, Thermo Fisher) of the used primary antibodies were prepared. After staining, cells were washed with PBS and stored on ice until acquisition. Acquisition was performed using BD FACSCanto TM II, BD LSR for analysis or Aria for cell sorting (BD Biosciences).

14

Experiments were analysed using FlowJo Software. Flow cytometer results in percentage were extrapolated to the total number of cells obtained from the cell counting.

Whole mount staining

The omentum was fixed for 1 hour in 1% PFA at room temperature and washed with PBS. Tissues were washed three times for 5 min with permeabilization buffer (PBS, 0.1% BSA and 0.2% Triton X-100) and treated with 0.5 mL blocking buffer (5% donkey serum diluted PBS-T) for 1 hour at room temperature. Primary antibodies, CD45 (BD 553076) and luciferase (ab185924), were diluted in PBS-T with 2% donkey serum. Next day, samples were washed three times with PBS- 0.3% Tween. Afterwards secondary antibodies (1:200) were incubated for 1 hour at room temperature, washed three times with PBS 0.3% Tween and incubated with DAPI (1:10.000) for 15 min. Next, samples were incubated with clearing solution (FUnGi: 60% glycerol (vol/vol), 2.5M fructose, 2.5M urea, 10mM Tris Base, 1.0mM EDTA) at 4 °C overnight. Coverslips were mounted with FUnGi clearing solution and imaged with a confocal microscope (LSM 710, Carl Zeiss). All images were processed with ZENblue software (Carl Zeiss, Germany). Average mean intensities per image were counted with ImageJ software (NIH, Bethesda, MD, USA).

Immunohistochemistry

Paraffin-embedded sections (3 μm) were de-paraffinized and re-hydrated in xylene and step-wise reductions in alcohol concentrations. H&E staining was performed according to standard protocols. Cytokeratin DAB and CD11b: antigen retrieval was performed at pH9 with citrate buffer. Primary antibodies CD11b (abcam, ab133357, 1:200), and Pan-cytokeratin (undiluted, ZUC001-125), diluted in blocking solution, were incubated at 4°C overnight. After washing, sections were incubated with secondary antibodies coupled with ZytoChem Plus (HRP) Polymer anti-mouse, (ZYTOMED, ZYT-ZUC050-006) and ZytoChem

1   Plus (AP) Polymer anti-rabbit, (ZYTOMED, ZYT-ZUC031-006) diluted in antibody diluent

2   (Cell Signaling) for one hour at room temperature. Afterwards, slides were treated with DAB

3   Substrat Chromogen, Zytomed, ZYT-DAB057 and AP Red Kit, Zytomed, ZUC001-125.

4   Immunofluorescence staining: primary antibodies: CD31 (Abcam, ab28364, 1:50), VCAM

5   (Vcam, ab134047, 1:200) and αSMA (Sigma-Aldrich, A5228, 1:200) were diluted in blocking

6   solution. Fluorophore-conjugated secondary antibodies (Thermo Fisher Scientific) were

7   diluted in antibody diluent (Cell Signaling) together with isolectin-B4 (Thermo Fisher

8   Scientific, I32450). Images were obtained with slide scanner (Zeiss Axio Sacn.Z1, Carl

9   Zeiss) and a confocal microscope (LSM 710, Carl Zeiss). All images were processed with

10 ZENblue software (Carl Zeiss, Germany). Image quantification were proceeded with ImageJ

11 software (NIH, Bethesda, MD, USA).

12

13 **Cell culture**

14

15 Murine cardiac ECs (MCEC) were purchased from tebu-bio and cultured on gelatin-

16 coated surfaces in in DMEM containing 1 g/L D-glucose, 5 % FCS, 5 % HEPES, 100

17 units/ml penicillin and 100 µg/ml streptomycin.

18 HUVEC were grown and maintained until passage 5 in Endopan-3 Growth Medium

19 containing 3% FCS and supplements (Pan-Biotech).

20 SK-OV-3 cells were kindly donated by Dr. Christiane Opitz (DKFZ, Heidelberg) and

21 cultured in DMEM containing 1 g/L D-glucose, 10 % FCS, 5 % HEPES, 100 units/ml

22 penicillin and 100 µg/ml streptomycin.

23 ID8-luc cells were kindly donated by provided by Prof. Frances Balkwill (Barts Cancer

24 Institute, London, UK) and cultured in DMEM containing 1 g/L D-glucose, 10 % FCS, 5 %

25 HEPES, 100 units/ml penicillin and 100 µg/ml streptomycin.

1   All cell culture experiments were performed in a laminar flow hood and cells cultured

2   at 37°C and 95% relative humidity and 5% CO_2. Cell culture were tested on a regularly basis

3   for mycoplasma contamination periodically and before injecting the tumour cells into the

4   mice.

5   To study the role of RBPJ in the regulation of Notch target genes, human umbilical

6   vein endothelial cells (HUVECs) were infected with lentivirus constructs for CRISPR/Cas9

7   (Addgene plasmid #52961, lentiCRISPR v2) induced knock-out for *Rbpj*[35]. After 48 hours,

8   cells were infected with adenovirus (LifeTechnologies; pAD/CMV-V5-DEST) overexpressing

9   GFP as control or N1ICD.

10

11   **Isolation of peripheral blood nuclear cells (PBMC) from buffy coats**

12   Human buffy coats were purchased from blood donation service DRK Mannheim,

13   Germany. Peripheral blood nuclear cells (PBMC) were isolated by gradient centrifugation

14   using Biocoll density solution (L6715; Biochrom). Human buffy coat was diluted 1:1 with PBS

15   and added to the Biocoll density solution. This mixture was centrifuged at 430g for 20 min at

16   room temperature. After centrifugation, the white intermediate phase containing leukocytes

17   was collected and washed with PBS. To perform a positive isolation of monocytes, CD14

18   MACS beads were used with the LS column (130-042-402; Milentyi Biotec). The isolation of

19   CD14$^+$ monocytes was performed following the manufacture's protocol.

20

21   **Transwell assay**

22   Human ovarian cancer cells were seeded at 100,000 cells/ml in 500 µl RPMI medium

23   without FCS for 48 hours. For the ECs monolayer, inserts were coated for 2 hours with 2

24   µg/ml fibronectin (1918-FN-02M; R&D Systems) in PBS. 50,000 human ECs (*RBPJ* knock-

25   out or shRNA for *CXCL2* (pLKO.1; Sigma Aldrich) and respective controls) were seeded on

1   top of the insert membrane for 48 hours. To analyse monocyte transmigration, 200,000

2   CD14$^+$ cells were stained with carboxyfluorescein succinimidyl ester (CSFE; ThermoFischer)

3   and added onto the endothelial monolayer. The transwell plate was incubated for 2 hours.

4   For the chemotaxis assay with the recombinant proteins, transmigration of 50,000 CD14$^+$

5   cells were analysed towards 60 ng/mL CXCL2 (PeproTech GmbH) in RPMI medium without

6   FCS for 30 min. After incubation, the remaining cell suspension in the upper well was

7   aspirated and the transwell was cleaned with a cotton swab. The migrated cells were fixed

8   with 4% PFA for 20 min at room temperature. Imaging of transwell was performed with Cell

9   Observer (Carl Zeiss). From each transwell five evenly spaced field picture were taken using

10   20x objective and analysis was performed with Image J software.

11

12   **Enzyme-linked Immunosorbent Assay (ELISA)**

13   Protein expression of CXCL2 (MIP-2) was quantified using an enzyme-linked

14   immunosorbent assay (ELISA; Abcam ab184862). Cell culture supernatant was collected

15   after 24 hours and ELISA was performed following the manufacture's protocol.

16

17   **Bone marrow-derived macrophages (BMDMs) differentiation**

18   Mouse macrophages were derived from the bone marrow of wild-type C57BL/6 mice.

19   Femurs and tibiae were flushed several times with DMEM and collected cells were

20   centrifuged. Bone marrow cells were suspended in media and seeded on 10 cm petri dishes

21   (Corning). To differentiate these cells into macrophages, 10 ng/ml M-CSF (PeproTech

22   GmbH) were added to Dulbecco's modified Eagle's medium (DMEM) (Thermo Fisher)

23   supplemented with 10% fetal calf serum (FCS) (Biochrom, UK). Differentiation occurred

24   within seven days. Cells were afterwards stimulated with indicated amount of recombinant

25   protein CXCL2 (250-15-20, PeproTech GmbH) in DMEM medium without FCS or

26   conditioned medium of endothelial cells.

1

2 **Immunostaining**

3   BMDMs were cultured in DMEM with 10% FCS (Biochrom, UK) and 250,000

4 cells/well were seeded into 24-well plates on top of coverslips. BMDMs were treated with 40

5 ng/mL CXCL2 (PeproTech GmbH) in DMEM without FCS for 72 hours. Cells were washed

6 with PBS and fixed with 4% PFA for 10 min. Then, the coverslips were washed three times

7 for 5 minutes with PBS, permeabilized with PBS with 0.1 % Triton X-100 for 10 minutes and

8 blocked for 30 min in blocking buffer (PBS in 5% FCS with 0.1% Tween 20 and 100 mM

9 glycine) for 1 hour at room temperature. The coverslips were incubated with antibody against

10 CD44 (1:1000) (Abcam, ab124515) and CD45 (1:500) (BD 553076) overnight at 4°C. The

11 coverslips were rinsed three times with blocking buffer and incubated with a secondary

12 antibody coupled to Alexa Fluor-488 and Alexa Fluor-546 (1:200) for 1 hour. The coverslips

13 were washed and incubated with a DAPI solution before they were washed again.

14 Coverslips were mounted and imaged with a confocal microscope (LSM 710, Carl Zeiss). All

15 images were processed with ZENblack software (Carl Zeiss, Germany).

16

17 **cDNA synthesis and qPCR**

18   RNA isolation from cell culture was performed using the InnuPrep Mini Kit (Analytik

19 Jena) according manufacture's protocol. RNA isolation form tissue was performed using

20 PicoPure RNA Isolation Kit (Acturus, Life Technology). 1 mL Trizol was added to the tissue

21 and homogenized for 1 min and a frequency of 30/sec. After disruption of the tissue, 200 µL

22 chloroform were added and mixed by inverting several times followed by a centrifugation

23 step for 15 minutes 12.000g at 4°C. Further RNA isolation steps were performed using the

24 manufacture's protocol. RNA concentration was measured using a Nanodrop 100 (Thermo

25 Fisher Scientific). Reverse transcription of isolated RNA into complementary DNA was

26 performed using High-Capacity cDNA Reverse Transcription Kit (Thermo Fisher Scientific).

1 Quantitative real-time PCR (qPCR) was performed with SYBR Green PCR mix (Applied

2 Biosystems) on a QuantStudio3 Real-time PCR system (Applied Biosystems). Resulting fold

3 changes were calculated using the $2^{\Delta\Delta CT}$ method and mRNA expression was normalized to

4 the housekeeping gene (*Cph* for murine and *HPRT* for human samples).

5 Primers used for mouse genes

Gene Name	Forward Primer	Reverse Primer
Cph	ATGGTCAACCCCACCGTG	TTCTTGCTGTCTTTGGAACTTTGTC
Ccl1	CTGCTGCTTGAACACCTTGA	GGTGATTTTGAACCCACGTT
Ccl21	ACCCAAGGCAGTGATGGA	CAGGGTTTGCACATAGCTCA
Cxcl2	CCAACCACCAGGCTACAGG	GCGTCACACTCAAGCTCTG
Cxcl12	GTCCTCTTGCTGTCCAGCTC	TAATTTCGGGTCAATGCACA
Cd44	TCGATTTGAATGTAACCTGCCG	CAGTCCGGGAGATACTGTAGC
Mmp9	CTGGACAGCCAGACACTAAAG	CTCGCGGCAAGTCTTCAGAG

6 Primers used for human genes

Gene Name	Forward Primer	Reverse Primer
HPRT	TGTTGTAGGATATGCCCTTGACT	CTAAGCAGARGGCCACAGAAC
CCL1	CATTTGCGGAGCAAGAGATT	TGCCTCAGCATTTTTCTGTG
CCL2	CAGCCAGATGCAATCAATGCC	TGGAATCCTGAACCCACTTCT
CCL21	CCCAGCTATCCTGTTCTTGC	TCAGTCCTCTTGCAGCCTTT
CXCL2	GGCAGAAAGCTTGTCTCAACCC	CTCCTTCAGGAACAGCCACCAA
CXCL5	AGCTGCGTTGCGTTTGTTTAC	TGGCGAACACTTGCAGATTAC
CXCL8	AAGAAACCACCGGAAGGAAC	AAATTTGGGGTGGAAAGGTT
CXCL12	ATTCTCAACACTCCAAACTGTGC	ACTTTAGCTTCGGGTCAATGC

7

8 **Cytotoxicity assay**

9 To analyse the T cell killing potential by the lactate dehydrogenase (LDH)-

10 Cytotoxicity Assay Kit (Ab65393, Abcam), ID8 cells (7,500 ID8 cells in 100 µL DMEM

11 medium) were seeded in a 96-well plate one day before T cell sorting. T cells were sorted

12 from tumour bearing $Rbpj^{i\Delta EC}$ and control mice after six weeks of tumour growth and 10,000

13 CD3$^+$ cells were co-cultured with ID8 cells in technical triplicates including untreated control

14 and blank. After overnight incubation, cytotoxicity and killing potential was measured by LDH

15 amount in the cell supernatant using the LDH-Cytotoxicity Assay Kit (Ab65393, Abcam)

16 following the manufacturer's protocol.

1

In silico analysis of promotor region

3   To determine RBPJ binding sites[36] (5´-GTGGGAA-3´) in the promotor region of the

4 murine (NM_009140; chr5+:90902580-90903927) and human (NM_002089; chr4-

5 :74100502-74099123) CXCL2-encoding gene, we used ApE plasmid Editor by M. Wayne

6 Davis (https://jorgensen.biology.utah.edu/wayned/ape/).

7

In silico protein-protein interaction

9   We used the Search Tool of Interacting Genes/Proteins database (STRING v11.5) to

10 perform *in silico* protein-protein interaction analysis[37]. Given CXCR2 protein as input,

11 STRING can search for their neighbour interactors, the proteins that have direct interactions

12 with the inputted proteins; then STRING can generate the PPI network consisting of all these

13 proteins and all the interactions between them. All the interactions between them were

14 derived from high-throughput lab experiments and previous knowledge in curated databases

15 at medium level of confidence (score ≥ 0.40).

16

Gene set enrichment analysis (GSEA)

18   GSEA (Broad Institute) was used to determine if a list of genes (gene signature) was

19 enriched between different groups. A defined list of genes exhibits a statistically significant

20 bias in their distribution (false discovery rate (FDR)) within a ranked gene list using the

21 software GSEA[38] resulting to an enrichment in one of the compared groups (normalized

22 enrichment score (NES)) obtained from microarray or public available data sets as indicated

23 in the figure legend.

24

Ingenuity Pathway Analysis (IPA)

1   IPA software (Qiagen) was used to identify predicated upstream regulators and

2   differentially regulated pathways in newly recruited macrophages (based on microarray

3   data). For the analysis of data, fold-changes were uploaded to the software. Differentially

4   regulated pathways and upstream regulator analysis was performed from obtained

5   microarray data.

6

7   Pathway analysis

8   Pathway analysis were obtained from public external databases (EnrichR) and

9   analysed as -2log fold changes.

10

11   Human ovarian cancer patient RNAseq data analysis

12   Human ovarian cancer patient bulk tumour RNA-sequencing data was obtained from

13   the Cancer Genome Atlas (TCGA) database. Stratification in $CXCL2^{high}$ and $CXCL2^{low}$

14   patients was performed using R Studio software. Patients were assigned to the different

15   groups using *CXCL2* expression below the first or higher than the third quartile. Normalised

16   raw counts of CD44 were plotted comparing the two different groups.

17

18   Statistical analysis

19   Normality was tested when sample size allowed it. Those samples with normal

20   distribution where compared using Students´ t-test (with Welch's correction when groups

21   had different sizes). When normality was rejected, Mann-Whitney U-test was used.

22   Comparison analysis was performed with analysis of variance (ANOVA) with Tukey post-test

23   when more than two groups were analysed. Statistical analysis and the generation of the

24   graphs were performed using GraphPad Prism 9 (GraphPad Software, Inc.; La Jolla, CA,

25   USA).

1

Schematic Figures

Schematics were created using BioRender.com.

4

Acknowledgements

23

Author Contributions

1   R.M., E.A-S, I.M., S.B., L.W., L.J., T.Z., J.T., F.A.R., A.S., B.D.G., J.R-V. performed

2   experiments. A.C., T.B., A.F. and J.R-V. contributed to analysis of results. A.F. and J.R-V.

3   conceived the original hypothesis. R.M., E.A-S, A.F. and J.R-V. planned experiments. R.M.,

4   E.A-S., J.R-V. and A.F. wrote the manuscript. J.R-V. directed and supervised the work.

5

6   **Competing Interests statement**

7   Authors declare that they have no competing interests.

8

9   **References**

10 1   Ferlay, J. *et al.* Cancer statistics for the year 2020: An overview. *Int J Cancer*,
11   doi:10.1002/ijc.33588 (2021).

12 2   Kipps, E., Tan, D. S. & Kaye, S. B. Meeting the challenge of ascites in ovarian cancer: new
13   avenues for therapy and research. *Nat Rev Cancer* **13**, 273-282, doi:10.1038/nrc3432 (2013).

14 3   Hensler, M. *et al.* M2-like macrophages dictate clinically relevant immunosuppression in
15   metastatic ovarian cancer. *J Immunother Cancer* **8**, doi:10.1136/jitc-2020-000979 (2020).

16 4   Goossens, P. *et al.* Membrane Cholesterol Efflux Drives Tumor-Associated Macrophage
17   Reprogramming and Tumor Progression. *Cell Metab* **29**, 1376-1389 e1374,
18   doi:10.1016/j.cmet.2019.02.016 (2019).

19 5   Noy, R. & Pollard, J. W. Tumor-associated macrophages: from mechanisms to therapy.
20   *Immunity* **41**, 49-61, doi:10.1016/j.immuni.2014.06.010 (2014).

21 6   Rafii, S., Butler, J. M. & Ding, B. S. Angiocrine functions of organ-specific endothelial cells.
22   *Nature* **529**, 316-325, doi:10.1038/nature17040 (2016).

23 7   Augustin, H. G. & Koh, G. Y. Organotypic vasculature: From descriptive heterogeneity to
24   functional pathophysiology. *Science* **357**, doi:10.1126/science.aal2379 (2017).

25 8   Alsina-Sanchis, E., Mulfarth, R. & Fischer, A. Control of Tumor Progression by Angiocrine
26   Factors. *Cancers (Basel)* **13**, doi:10.3390/cancers13112610 (2021).

27 9   Zhao, Q. *et al.* Single-Cell Transcriptome Analyses Reveal Endothelial Cell Heterogeneity in
28   Tumors and Changes following Antiangiogenic Treatment. *Cancer Res* **78**, 2370-2382,
29   doi:10.1158/0008-5472.CAN-17-2728 (2018).

30 10   Zhao, Q. *et al.* Heterogeneity and chimerism of endothelial cells revealed by single-cell
31   transcriptome in orthotopic liver tumors. *Angiogenesis* **23**, 581-597, doi:10.1007/s10456-
32   020-09727-9 (2020).

33 11   Wieland, E. *et al.* Endothelial Notch1 Activity Facilitates Metastasis. *Cancer Cell* **31**, 355-367,
34   doi:10.1016/j.ccell.2017.01.007 (2017).

35 12   Bray, S. J. Notch signalling in context. *Nat Rev Mol Cell Biol* **17**, 722-735,
36   doi:10.1038/nrm.2016.94 (2016).

37 13   Limbourg, F. P. *et al.* Essential role of endothelial Notch1 in angiogenesis. *Circulation* **111**,
38   1826-1832, doi:10.1161/01.CIR.0000160870.93058.DD (2005).

39 14   Hasan, S. S. *et al.* Endothelial Notch signaling controls insulin transport in muscle. *EMBO Mol*
40   *Med* **12**, e09271, doi:10.15252/emmm.201809271 (2020).

15   Ramasamy, S. K., Kusumbe, A. P., Wang, L. & Adams, R. H. Endothelial Notch activity promotes angiogenesis and osteogenesis in bone. *Nature* **507**, 376-380, doi:10.1038/nature13146 (2014).

16   Sorensen, I., Adams, R. H. & Gossler, A. DLL1-mediated Notch activation regulates endothelial identity in mouse fetal arteries. *Blood* **113**, 5680-5688, doi:10.1182/blood-2008-08-174508 (2009).

17   Jabs, M. *et al.* Inhibition of Endothelial Notch Signaling Impairs Fatty Acid Transport and Leads to Metabolic and Vascular Remodeling of the Adult Heart. *Circulation* **137**, 2592-2608, doi:10.1161/CIRCULATIONAHA.117.029733 (2018).

18   Zhu, T. S. *et al.* Endothelial cells create a stem cell niche in glioblastoma by providing NOTCH ligands that nurture self-renewal of cancer stem-like cells. *Cancer Res* **71**, 6061-6072, doi:10.1158/0008-5472.CAN-10-4269 (2011).

19   Etzerodt, A. *et al.* Tissue-resident macrophages in omentum promote metastatic spread of ovarian cancer. *J Exp Med* **217**, doi:10.1084/jem.20191869 (2020).

20   Verginelli, F. *et al.* Activation of an endothelial Notch1-Jagged1 circuit induces VCAM1 expression, an effect amplified by interleukin-1beta. *Oncotarget* **6**, 43216-43229, doi:10.18632/oncotarget.6456 (2015).

21   Jablonska, J., Wu, C. F., Andzinski, L., Leschner, S. & Weiss, S. CXCR2-mediated tumor-associated neutrophil recruitment is regulated by IFN-beta. *Int J Cancer* **134**, 1346-1358, doi:10.1002/ijc.28551 (2014).

22   Taki, M. *et al.* Snail promotes ovarian cancer progression by recruiting myeloid-derived suppressor cells via CXCR2 ligand upregulation. *Nat Commun* **9**, 1685, doi:10.1038/s41467-018-03966-7 (2018).

23   Gilliver, S. C., Emmerson, E., Bernhagen, J. & Hardman, M. J. MIF: a key player in cutaneous biology and wound healing. *Exp Dermatol* **20**, 1-6, doi:10.1111/j.1600-0625.2010.01194.x (2011).

24   Alban, T. J. *et al.* Glioblastoma Myeloid-Derived Suppressor Cell Subsets Express Differential Macrophage Migration Inhibitory Factor Receptor Profiles That Can Be Targeted to Reduce Immune Suppression. *Front Immunol* **11**, 1191, doi:10.3389/fimmu.2020.01191 (2020).

25   Shi, X. *et al.* CD44 is the signaling component of the macrophage migration inhibitory factor-CD74 receptor complex. *Immunity* **25**, 595-606, doi:10.1016/j.immuni.2006.08.020 (2006).

26   Priego, N. *et al.* STAT3 labels a subpopulation of reactive astrocytes required for brain metastasis. *Nat Med* **24**, 1024-1035, doi:10.1038/s41591-018-0044-4 (2018).

27   Cortes, M. *et al.* Tumor-associated macrophages (TAMs) depend on ZEB1 for their cancer-promoting roles. *EMBO J* **36**, 3336-3355, doi:10.15252/embj.201797345 (2017).

28   Figueiredo, C. R. *et al.* Blockade of MIF-CD74 Signalling on Macrophages and Dendritic Cells Restores the Antitumour Immune Response Against Metastatic Melanoma. *Front Immunol* **9**, 1132, doi:10.3389/fimmu.2018.01132 (2018).

29   Przybyl, L. *et al.* CD74-Downregulation of Placental Macrophage-Trophoblastic Interactions in Preeclampsia. *Circ Res* **119**, 55-68, doi:10.1161/CIRCRESAHA.116.308304 (2016).

30   Moughon, D. L. *et al.* Macrophage Blockade Using CSF1R Inhibitors Reverses the Vascular Leakage Underlying Malignant Ascites in Late-Stage Epithelial Ovarian Cancer. *Cancer Res* **75**, 4742-4752, doi:10.1158/0008-5472.CAN-14-3373 (2015).

31   Zhang, F., Jiang, J., Xu, B., Xu, Y. & Wu, C. Over-expression of CXCL2 is associated with poor prognosis in patients with ovarian cancer. *Medicine (Baltimore)* **100**, e24125, doi:10.1097/MD.0000000000024125 (2021).

32   Di Mitri, D. *et al.* Re-education of Tumor-Associated Macrophages by CXCR2 Blockade Drives Senescence and Tumor Inhibition in Advanced Prostate Cancer. *Cell Rep* **28**, 2156-2168 e2155, doi:10.1016/j.celrep.2019.07.068 (2019).

33   Henriques, T. B. *et al.* Inhibition of CXCR2 plays a pivotal role in re-sensitizing ovarian cancer to cisplatin treatment. *Aging (Albany NY)* **13**, 13405-13420, doi:10.18632/aging.203074 (2021).

34   Alsina-Sanchis, E. *et al.* Intraperitoneal Oil Application Causes Local Inflammation with Depletion of Resident Peritoneal Macrophages. *Mol Cancer Res* **19**, 288-300, doi:10.1158/1541-7786.MCR-20-0650 (2021).

35   Sanjana, N. E., Shalem, O. & Zhang, F. Improved vectors and genome-wide libraries for CRISPR screening. *Nat Methods* **11**, 783-784, doi:10.1038/nmeth.3047 (2014).

36   Lake, R. J., Tsai, P. F., Choi, I., Won, K. J. & Fan, H. Y. RBPJ, the major transcriptional effector of Notch signaling, remains associated with chromatin throughout mitosis, suggesting a role in mitotic bookmarking. *PLoS Genet* **10**, e1004204, doi:10.1371/journal.pgen.1004204 (2014).

37   Szklarczyk, D. *et al.* The STRING database in 2021: customizable protein-protein networks, and functional characterization of user-uploaded gene/measurement sets. *Nucleic Acids Res* **49**, D605-D612, doi:10.1093/nar/gkaa1074 (2021).

38   Subramanian, A. *et al.* Gene set enrichment analysis: a knowledge-based approach for interpreting genome-wide expression profiles. *Proc Natl Acad Sci U S A* **102**, 15545-15550, doi:10.1073/pnas.0506580102 (2005).

39   de Vos van Steenwijk, P. J. *et al.* Tumor-infiltrating CD14-positive myeloid cells and CD8-positive T-cells prolong survival in patients with cervical carcinoma. *Int J Cancer* **133**, 2884-2894, doi:10.1002/ijc.28309 (2013).
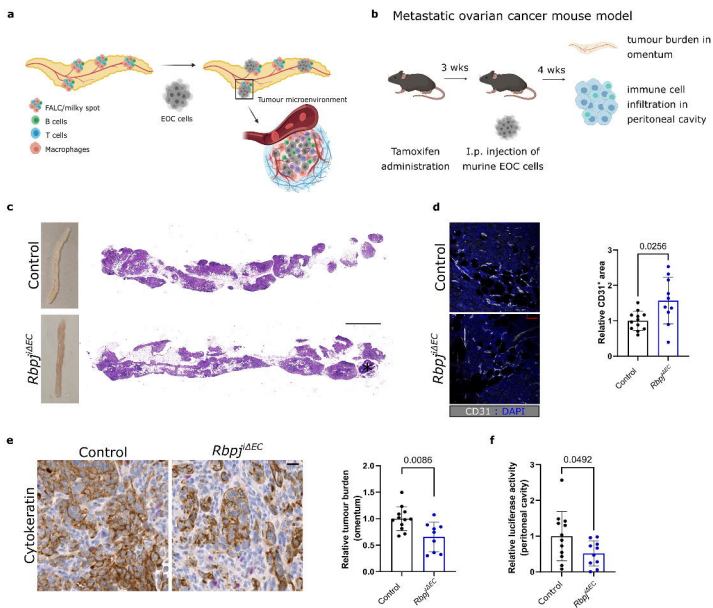
a

FALC/milky spot
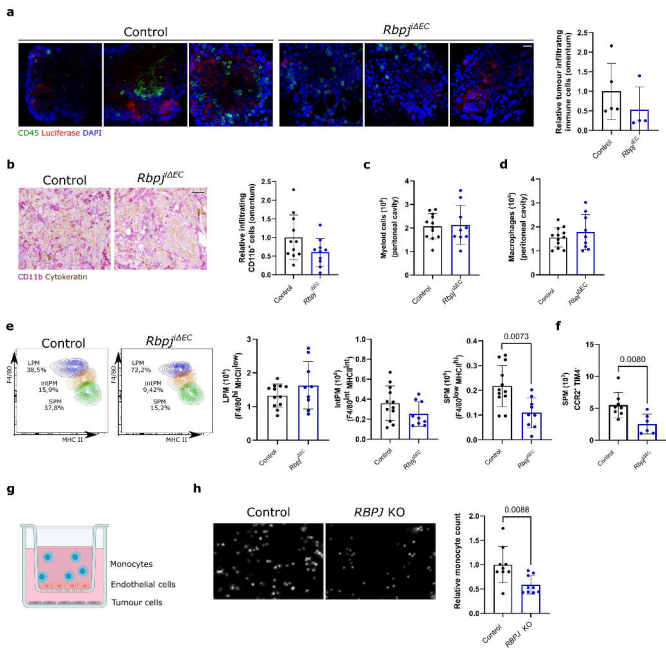B cells
T cells
Macrophages

EOC cells

Tumour microenvironment

b Metastatic ovarian cancer mouse model

3 wks → 4 wks

tumour burden in omentum

immune cell infiltration in peritoneal cavity

Tamoxifen administration

I.p. injection of murine EOC cells

c

Control

$Rbpj^{\Delta EC}$

d

Control

$Rbpj^{\Delta EC}$

CD31 : DAPI

0.0256

Relative CD31+ area

Control $Rbpj^{\Delta EC}$

e

Control $Rbpj^{\Delta EC}$

Cytokeratin

0.0086

Relative tumour burden (omentum)

Control $Rbpj^{\Delta EC}$

f

0.0492

Relative luciferase activity (peritoneal cavity)

Control $Rbpj^{\Delta EC}$

Figure 1.

a

Control   *Rbpj^iΔEC*

CD45 Luciferase DAPI

b

Control   *Rbpj^iΔEC*

CD11b Cytokeratin

c

d

e

Control   *Rbpj^iΔEC*

LPM 36.5%   LPM 72.2%
intPM 15.9%   intPM 0.42%
SPM 37.8%   SPM 1.2%

f

g

Monocytes
Endothelial cells
Tumour cells

h

Control   *RBPJ* KO

Figure 2.

Figure 3.

Figure 4.

Figure 5.

a

b ID8 TAM-signature - IL4-treated BMDMs

c CD74-mediated signature -CCR2⁺

d Cytotoxicity assay from tumour-bearing mice sorted T cells

e

f

g

Figure 6.